# An analytical model for direct initiation of gaseous detonations

**C.A. Eckett, J.J. Quirk, J.E. Shepherd**

Graduate Aeronautical Laboratories, California Institute of Technology, Pasadena CA 91125, USA

**Abstract:** A new model is presented for direct initiation of gaseous detonations by a blast wave. The analysis identifies unsteadiness in the induction zone as the primary physical mechanism by which a detonation may fail to initiate. The local model of the reaction zone is verified by numerical simulations and then used to produce an equation for the critical energy which agrees with empirical correlations to within an order of magnitude.

**Key words:** Detonation, Detonation initiation, Computational fluid dynamics

## 1. Introduction

When a large amount of energy is released in a small region of an unconfined combustible gas mixture, the ensuing spherical blast wave can initiate a spherical detonation in the gas. In other cases, a detonation is not initiated and the blast wave decays away to an acoustic wave in the manner of a blast in a non-reacting gas. The main factor believed to control this initiation event is the initial energy release. Experiments suggest that it must be above a certain level, known as the critical energy, to successfully initiate a detonation. Experimental correlations have typically assumed that the critical energy $E_c$ can be well approximated by

$$E_c = B\rho_0 U_{CJ}{}^2 \lambda^3,$$

where $\rho_0$ is the initial gas density, $U_{CJ}$ is the Chapman-Jouget (CJ) velocity, and $\lambda$ is the detonation cell width. Our correlation of experimental data presented in Benedick et al. (1986) suggests that the constant $B \approx 200$. Assuming the cell width is roughly related to the induction zone length $\Delta_i$ by $\lambda \approx 30\Delta_i$ then gives,

$$E_c = B'\rho_0 U_{CJ}{}^2 \Delta_i{}^3,$$

where the proportionality constant $B' \approx 5 \times 10^6$.

Various attempts have been made in the past to derive an equation for the critical energy (see Lee (1977) and Benedick et al. (1986)), but these were phenomenological models that simply attempted to relate the critical energy $E_c$ to other experimentally determined dynamic parameters such as the cell width $\lambda$ or the critical tube diameter $d_c$. There is certainly value to this, since these other parameters are easier to measure experimentally, but there exists no satisfactory model for predicting $\lambda$

or $d_c$ so the real physics in the initiation problem is left unexplained. A recent attempt to find a more fundamental model was made by He and Clavin (1994), who considered the influence of the leading shock curvature on initiation problems to be the fundamental issue.

Here we present an alternative idea which suggests unsteadiness in the reaction zone is the dominant mechanism causing direct initiation failure. Analysis of the 1D reaction zone structure leads us to a local initiation model in Section 2, which we verify through direct numerical simulations in Section 3. The local model is then used in Section 4 to produce a global model which gives satisfactory predictions for critical energy.

## 2. Local initiation model

The starting equations are the mass, momentum and species conservation equations of the spherically symmetric reactive Euler equations,

$$\frac{D\rho}{Dt} + \rho\frac{\partial u}{\partial r} + \frac{2}{r}\rho u = 0, \qquad (1)$$

$$\frac{Du}{Dt} + \frac{1}{\rho}\frac{\partial P}{\partial r} = 0, \qquad (2)$$

$$\frac{Dy_i}{Dt} = \Omega_i, \qquad (3)$$

where $u$, $\rho$ and $P$ are the velocity, density and pressure, $r$ is the distance from the coordinate origin, $t$ is the time, $y_i$ is the mass fraction of species $i$, and $\Omega_i$ is the rate of production of species $i$. The energy equation is replaced by the adiabatic change equation, from Fickett and Davis (1979),

$$\frac{DP}{Dt} = c^2\frac{D\rho}{Dt} + \rho c^2\dot{\sigma}, \qquad (4)$$

where $c$ is the frozen sound speed, $\dot{\sigma} = \sum \sigma_i \Omega_i$ is the total thermicity, and $\sigma_i$ is the thermicity coefficient of species $i$. These equations can be transformed to the frame of reference of the leading shock,

$$x = R(t) - r, \quad w(x,t) = U(t) - u(r,t),$$

where $R$ and $U$ are the position and velocity of the shock, and $w$ is the flow velocity in the shock-fixed reference frame. They can then be rearranged to give the following

reaction zone structure equations:

$$\eta \frac{Dw}{Dt} = w\dot{\sigma} - \frac{2}{R-x}(U-w)w$$
$$- M^2 \frac{dU}{dt} + \frac{\partial w}{\partial t} - \frac{w}{\rho c^2}\frac{\partial P}{\partial t}, \qquad (5)$$

$$\eta \frac{D\rho}{Dt} = -\rho\dot{\sigma} + \frac{2}{R-x}(U-w)\rho M^2$$
$$+ \frac{\rho w}{c^2}\frac{dU}{dt} - \frac{\rho w}{c^2}\frac{\partial w}{\partial t} + \frac{1}{c^2}\frac{\partial P}{\partial t}, \qquad (6)$$

$$\eta \frac{DP}{Dt} = -\rho w^2\dot{\sigma} + \frac{2}{R-x}(U-w)\rho w^2$$
$$+ \rho w\frac{dU}{dt} - \rho w\frac{\partial w}{\partial t} + \frac{\partial P}{\partial t}, \qquad (7)$$

where $M = w/c$ is the Mach number, and $\eta$ is the sonic parameter $1 - M^2$. These equations are the solutions for the flow gradients along a particle path in the reaction zone. In each equation, the first term on the right hand side is the contribution from the chemical heat release, the second is that due to wave curvature, and the remaining terms represent the purely unsteady contribution.

If detonation failure is thought of as the failure of particles to rapidly undergo reaction after crossing the shock, then since the reaction rate is typically strongly dependent on temperature, the Lagrangian gradient of temperature will be of most interest in identifying detonation failure. Here we assume the simplest possible reaction, a one-step irreversible reaction, A $\rightarrow$ B, where A and B are perfect gases with the same molecular weight. Define the reaction progress variable $Z$ as the mass fraction of product B. Then the temperature reaction zone structure equation can be found:

$$\eta C_P \frac{DT}{Dt} = (1 - \gamma M^2)q\frac{DZ}{Dt}$$
$$+ \frac{2}{R-x}(U-w)w^2 \qquad (8)$$
$$+ w\frac{dU}{dt} - w\frac{\partial w}{\partial t} + \frac{1}{\rho}\frac{\partial P}{\partial t},$$

where $T$ is the temperature, $C_P$ is the specific heat at constant pressure, $\gamma$ is the ratio of specific heats, and $q$ is the heat of reaction. For a decelerating wave such as the blast wave in a spherical initiation problem, the unsteady terms in this equation will be of opposite sign to the heat release term, and will hence act to quench the reaction if the wave is decelerating too rapidly. For a convex wavefront such as a spherical wave, the curvature term in Eq. (8) is actually of the same sign as the heat release term and so cannot possibly quench the detonation. As will be demonstrated in the following section, the curvature term is typically small compared

with the unsteady terms. We will ignore it in the subsequent analysis.

The kinetics are assumed to be governed by a first-order Arrhenius rate law,

$$\frac{DZ}{Dt} = k(1-Z)\exp\left(-\frac{E_a}{R_g T}\right), \qquad (9)$$

where $R_g$ is the specific gas constant, $E_a$ is the activation energy, and $k$ is the pre-exponential rate multiplier.

Assuming a large activation energy, asymptotic expansions of the flow variables can be made in the induction zone using the parameter $\theta = E_a/R_g T_s$, where subscript $s$ refers to conditions immediately after the shock. For example, $T/T_s = 1 + \phi/\theta + O(1/\theta^2)$. If the time scale of evolution of the partial time derivatives in Eq. (8) is much greater than the induction time (the time scale in the Lagrangian derivative), the leading order asymptotic equation is,

$$\eta_s C_P T_s \frac{1}{\theta}\frac{D\phi}{Dt} = (1 - \gamma M_s^2)qke^{\phi-\theta} \qquad (10)$$
$$+ w_s\frac{dU}{dt} - w_s\frac{dw_s}{dt} + \frac{1}{\rho_s}\frac{dP_s}{dt}.$$

The unsteady terms are now a prescribed forcing, and we have reduced the equation from a PDE to an ODE which can be solved analytically. It is found that thermal runaway ($\phi \rightarrow \infty$) occurs in finite time provided

$$-\frac{\theta w_s t_i}{\eta_s C_P T_s}\left(\frac{dU}{dt} - \frac{dw_s}{dt} + \frac{1}{\rho_s w_s}\frac{dP_s}{dt}\right) < 1, \qquad (11)$$

where

$$t_i = \frac{1}{k}\frac{1 - M_s^2}{1 - \gamma M_s^2}\frac{1}{\theta}\frac{C_P T_s}{q}e^{\theta} \qquad (12)$$

is the asymptotic induction time for a planar ZND wave. We refer to the left hand side of Eq. (11) as the initiation parameter $\alpha$, so the critical initiation parameter is $\alpha_c = 1$. The expression for $\alpha_c$ can be simplified using the strong shock jump conditions. Defining a characteristic shock decay time $t^*$ by

$$\frac{1}{t^*} \equiv -\frac{1}{U}\frac{dU}{dt},$$

we then find the critical shock decay time is

$$t_c^* = 6\frac{\gamma - 1}{\gamma + 1}\theta t_i. \qquad (13)$$

This indicates $t_c^*$ is proportional to the detonation induction time, as expected from dimensional analysis. Since $\theta$ is large, Eq. (13) also demonstrates that unsteadiness can be important even when $t^* \gg t_i$. It is only when $t^* \gg \theta t_i$ that the unsteady terms can be neglected and the flow considered quasi-steady.

## 3. Numerical simulations

### 3.1. Computational details

To examine the governing physical processes and validate the model, we performed direct numerical simulations of point-initiated spherical detonations. All computations were performed with the irreversible one-step mechanism considered in the previous section. The spherically symmetric reactive Euler equations were written in conservative form, in a fixed reference frame. Normalization was made by the upstream conditions for density, pressure and temperature, $u_{ref} = \sqrt{R_g T_0}$ for velocity, the half reaction length $\Delta$ for length, and $t_{ref} = \Delta/u_{ref}$ for time.

Integration was performed using operator splitting. The convective flux was integrated with Roe's approximate Riemann solver (Roe 1986), using a general equation of state implementation due to Glaister (1988). Second-order accuracy was obtained via Min-Mod flux limiting. The integration of the geometry source terms was by first-order forward Euler, while the reaction source terms were integrated by a nominally second-order predictor-corrector scheme. The code was incorporated in the Amrita CFD programming system of Quirk (1997), making use of an adaptive mesh refinement algorithm (Quirk 1991). Sufficient refinement was used at the leading shock and in the reaction zone to capture a finely resolved shock and have at least 100 grid cells in the reaction zone.

The results presented in this paper use the following fluid and chemical parameters:

$$\gamma = 1.4, \quad q = 12\, R_g T_0, \quad E_a = 25\, R_g T_0.$$

This corresponds to a marginally unstable planar CJ detonation, based on the normal mode 1D stability analysis of Lee and Stewart (1990). A higher activation energy would better approximate real gas mixtures and would result in a more square-wave type structure as assumed in the asymptotics. However, He (1996) has shown that for high activation energies, the gross instability characteristics of the one-step model cause failure of the wave for any igniter energy, a property not indicative of real flows. The same paper also demonstrated that even for slightly unstable mixtures, the instability provides a secondary, weaker mechanism of detonation failure. To isolate only the primary fluid dynamic mechanism, we decided to stay near the stability boundary. Various other parameter sets were investigated in the vicinity of the stability boundary, varying $\gamma$ between 1.2 and 1.6, and $q/R_g T_0$ between 8 and 33. The behavior of the parameter set considered here appears to be universal in the ranges studied. The chosen parameters give the following CJ detonation:

$$U_{CJ} = 5.08\, u_{ref}, \quad P_{CJ} = 11.2\, P_0, \quad P_{vN} = 21.3\, P_0,$$

where subscript $vN$ refers to the von Neumann conditions (post-shock state) in a CJ detonation.

The initial conditions used were a small, motionless, high pressure hot core of fully reacted gas centered at the origin, so the problem was effectively that of a spherical shock tube. The conditions of the core were chosen to approximate the energy density and temperature of a typical high explosive. Table 1 shows the core initial conditions and size for the three cases presented. The

**Table 1.** Initial conditions for numerical simulations.

|  | Case A | Case B | Case C |
|---|---|---|---|
| $r_{core}/\Delta$ | 6.30 | 10.00 | 15.87 |
| $P_{core}/P_0$ | $2 \times 10^4$ | $2 \times 10^4$ | $2 \times 10^4$ |
| $\rho_{core}/\rho_0$ | $2 \times 10^3$ | $2 \times 10^3$ | $2 \times 10^3$ |
| $E_{source}/P_0\Delta^3$ | $5.24 \times 10^7$ | $2.09 \times 10^8$ | $8.38 \times 10^8$ |

source energy $E_{source}$ increases by a factor of 4 in each case. Variation of the initial conditions revealed that the core pressure was high enough such that the flow was approximately independent of the exact form of energy deposition, by the time the blast wave had decayed to the CJ velocity. So the igniter may be considered a point source.

### 3.2. Computational results

Figure 1 shows a time series of spatial pressure profiles, for cases B and C. Case B decays to slightly below CJ velocity, re-accelerates briefly, but then fails and decays away like a non-reacting blast wave. The disappearance of the von Neumann spike is evident. Case C successfully initiates and forms a spherically expanding detonation at close to CJ conditions. The velocity of the leading shock wave is shown in Fig. 2 for all three cases. Case B is a marginal failure between the failure and successful initiation of cases A and C respectively. The hump in the velocity profile of case B is a manifestation of the instability of the detonation. It was not observed in runs with stable mixtures. Figure 3 shows the location of the leading shock and the points of 5% and 95% reaction completion, on an $r$-$t$ plot for case B. The point of failure where the reaction zone decouples from the shock is clearly evident around $t/t_{ref} = 67$. Also shown on this plot is the location of the sonic surface. A sonic point far behind the reaction zone is somewhat meaningless since the flow velocity there is clearly not related to the shock reference frame, but the region where the sonic surface penetrates the back of the reaction zone is relevant. While we do not propose that it controls the detonation failure, it is a good indicator of the state of the flow. Without a sonic point, the flow at the rear of the reaction zone is subsonic, and signals from the inner expansion wave can propagate into the reaction zone,
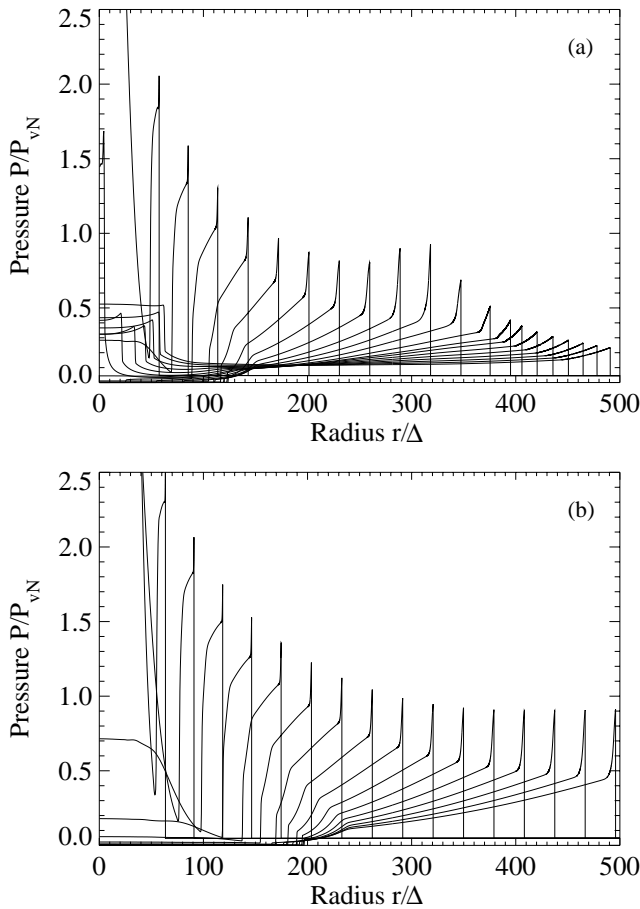
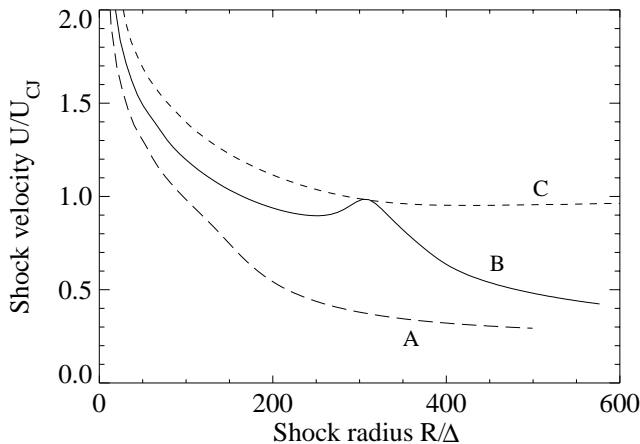Figure 1. Spatial pressure profiles at nearly equal time intervals. (a) Case B; (b) Case C.



Figure 2. Leading shock velocity versus radius for the three cases.

decelerating the shock.

### 3.3. Validation of local initiation model

The local initiation model suggested that information along particle paths in the reaction zone would be instru-
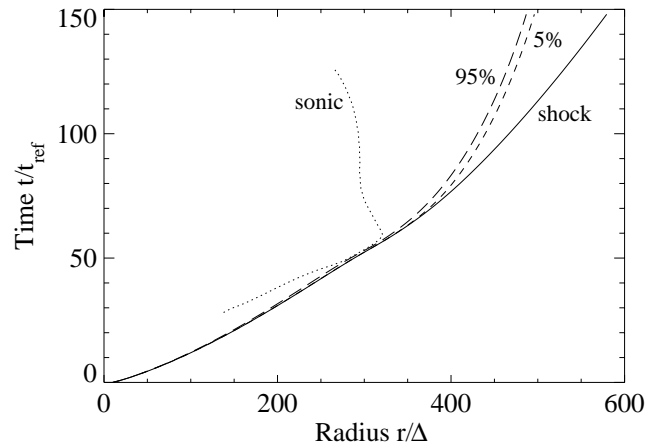


Figure 3. Location of shock, 5% and 95% reaction surfaces, and sonic point, for case B.

mental in determining initiation failure. Thus streamline data was extracted from the numerical output by interpolation of the flow field. Figure 4 shows the paths of ten
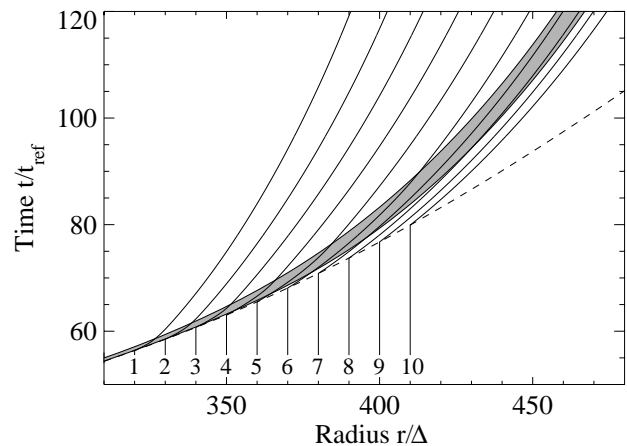


Figure 4. Ten sample particle paths for case B. Shock (dashed line); 5% to 95% reaction (shaded region); particle paths (solid lines).

sample particles from case B, in a magnified view of the critical region of Fig. 3. Also shown are the shock and partial reaction region. The first few particles rapidly pass through the reaction zone, indicating that the flow is still detonating at this stage. By about the fifth or sixth particle, the time taken to traverse the reaction zone becomes much longer, suggesting that the wave is failing. This is the same point at which the reaction zone decouples from the shock, so both concepts of failure lead to the same conclusion on when the detonation fails. The last two particles do not react at all in the time plotted, indicating that the reaction has completely quenched by then. The temperature profiles along the same ten particle paths are plotted in Fig. 5. Again it is clear that by particle path 5 or 6, the thermal explosion time is
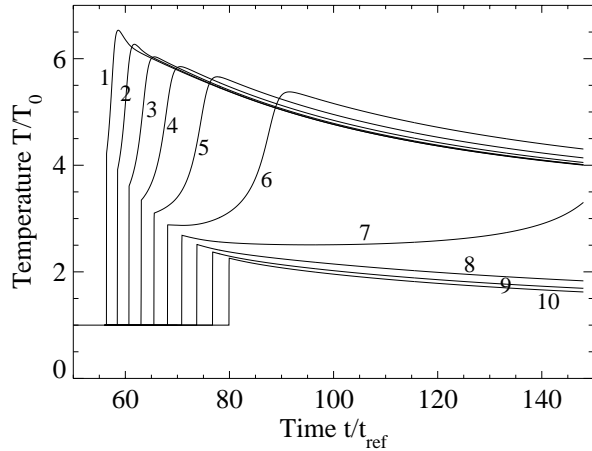
**Figure 5.** Temperature along same ten particle paths as in Fig. 4, for case B.

increasing rapidly. The last few particles do not reach thermal explosion at all in the computed time range. The slight negative temperature gradient after crossing the shock is the forcing of the unsteadiness, as discussed in the analysis of Section 2, and it is this gradient that prevents the later particles from exploding.

Figure 6 shows an extraction of the various contributions to the Lagrangian temperature gradient in Eq. (8), along two of the earlier particle paths. The time $t_p$ is measured from when each particle crosses the shock. In both cases, the curvature contribution is very small, justifying our earlier assumption that it can be safely ignored. Along particle path 4, the unsteadiness is a negative forcing that reduces the temperature gradient below that simply due to heat release, but it is not strong enough to prevent reaction. By particle path 7, the unsteadiness dominates the heat release, causing the total gradient to become negative for a considerable time, and the reaction essentially quenches. Notice that early in the reaction zone the unsteady terms are not strictly constant. This is because the one-step mechanism does not produce a real induction zone at the low activation energy used. It is expected that computations with real mixtures would better agree with the asymptotics.

As a final validation of the local model, the initiation parameter $\alpha$ is plotted in Fig. 7 for the two failed cases, cases A and B. Indeed, $\alpha$ is well below the critical value of 1 early in the flow, but then increases sharply upon failure. The time where $\alpha = 1$ in case B very closely matches the time of failure identified earlier.

## 4. Global initiation model

To convert the present local initiation model into a useful predictive formula for critical energy requires an *a priori* knowledge of the approximate blast wave velocity profile. The simplest choice is the Taylor-Sedov similarity
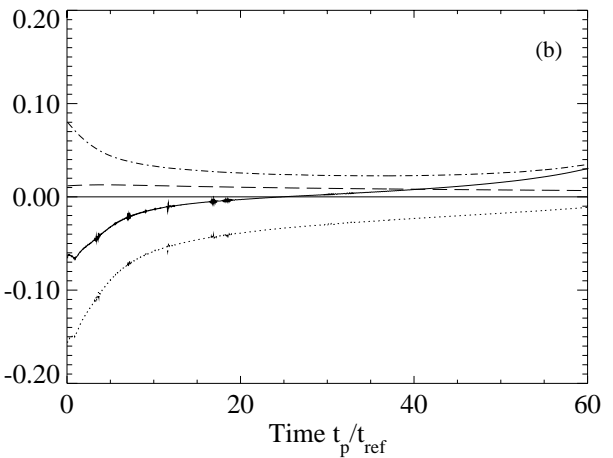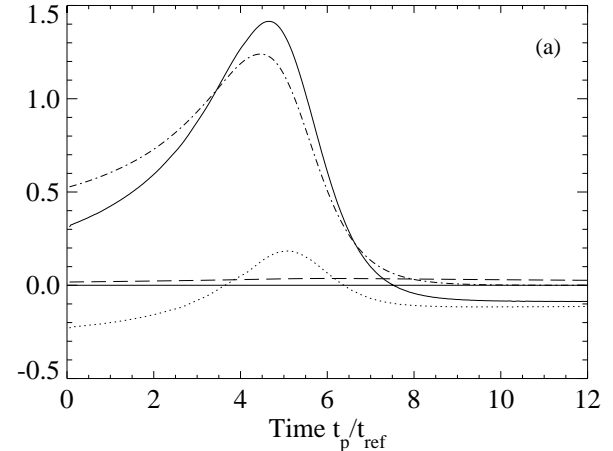


**Figure 6.** Terms in reaction zone temperature Eq. (8), for case B. —— total temperature gradient; $- \cdot - \cdot -$ heat release; $- - -$ curvature; $\cdots$ unsteadiness. (a) Particle 4; (b) Particle 7.
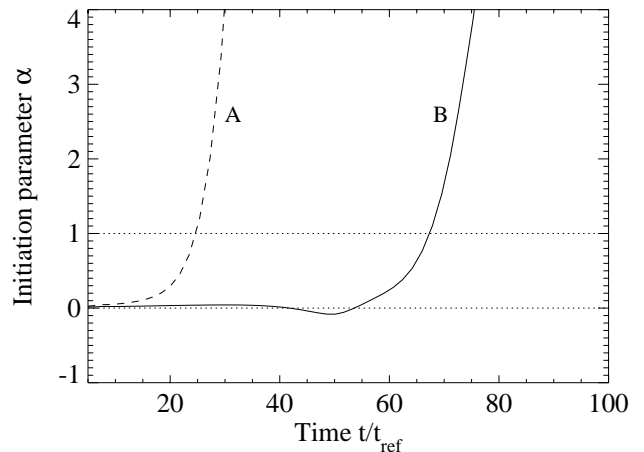


**Figure 7.** Initiation parameter $\alpha$ for cases A and B.

solution for a non-reacting strong point blast,

$$R = \left( \frac{E_{source}}{A \rho_0} \right)^{1/5} t^{2/5}, \qquad (14)$$

where $E_{source}$ is the igniter energy release, and $A$ is a blast wave constant which is a function only of $\gamma$ and is $O(1)$. Successive differentiation of this relation gives the characteristic shock decay time as

$$t^* = -\frac{U}{dU/dt} = \left(\frac{32}{675}\frac{E_{source}}{A\rho_0}\frac{1}{U^5}\right)^{1/3}. \qquad (15)$$

A further decision to make is at what point in the blast wave profile to apply the failure criterion. The numerical simulations suggest that these detonations typically fail around the point where the blast wave has decayed to the CJ velocity, so we will apply the model at $U = U_{CJ}$. Substituting Eq. (15) into Eq. (13), and introducing the asymptotic induction length for a planar detonation $\Delta_i = w_s t_i$ with the strong shock limit for $w_s$, gives the critical energy,

$$E_c = 4.56 \times 10^3 A\,\theta_{CJ}^{\,3}\rho_0 U_{CJ}^{\,2}\Delta_{i,CJ}^{\,3}. \qquad (16)$$

This equation has the same functional dependence on density, velocity and reaction zone length as the empirical relation in Section 1. For typical mixtures of hydrogen or hydrocarbons in air or oxygen, $\theta \approx 5$ to $15$, resulting in a constant of proportionality $B'$ of the order $10^6$ to $10^7$. This concurs with the previously proposed empirical relation.

## 5. Conclusions

We have demonstrated that in direct initiation of gaseous detonations by an overdriven blast wave, the primary physical mechanism by which a detonation may fail to initiate is unsteadiness in the reaction zone. This notion has been derived analytically by detailed consideration of the reaction zone structure, namely the competition between chemical heat release, wave curvature and flow unsteadiness. Direct numerical simulations have been used to confirm that heat release and unsteadiness form the dominant balance in the reaction zone structure temperature gradient equation, thus indicating excessive unsteadiness can cause quenching of the reaction and failure of the detonation to initiate.

## References

Benedick WB, Guirao CM, Knystautus R, Lee JH (1986) Critical charge for the direct initiation of detonation in gaseous fuel-air mixtures. Prog Astro Aero 106:181–202

Fickett W, Davis WC (1979) Detonation. University of California Press, Berkeley

Glaister P (1988) An approximate linearised Riemann solver for the Euler equations for real gases. J Comp Phys 74:382–408

He L (1996) Theoretical determination of the critical conditions for the direct initiation of detonations in hydrogen-oxygen mixtures. Comb Flame 104:401–418

He L, Clavin P (1994) On the direct initiation of gaseous detonations by an energy source. J Fluid Mech 277:227–248

Lee HI, Stewart DS (1990) Calculation of linear detonation instability: One-dimensional instability of plane detonation. J Fluid Mech 216:103–132

Lee JHS (1977) Initiation of gaseous detonation. Ann Rev Phys Chem 28:75–104

Quirk JJ (1991) An adaptive grid algorithm for computational shock hydrodynamics. PhD thesis, Coll of Aero, Cranfield Inst Tech, UK

Quirk JJ (1997) An introduction to Amrita. http://www.amrita-cfd.com

Roe PL (1986) Characteristic-based schemes for the Euler equations. Ann Rev Fluid Mech 18:337–365

▷ PREVIOUS PAPER

▷ NEXT PAPER

▷ CURRENT LOCATION IN TABLE OF CONTENTS

▷ CURRENT LOCATION IN REFERENCE NUMBER INDEX

▷ TOP OF TABLE OF CONTENTS

▷ TOP OF KEYWORDS INDEX

▷ TOP OF AUTHOR INDEX

▷ TOP OF REFERENCE NUMBER INDEX